Multi-instrumental monitoring of snowmelt infiltration in Vallon de Nant, Swiss Alps

Judith Eeckman[1], Brian De Grenus[2], Floreana Marie Miesen[2], James Thornton[4], Philip Brunner[5], and Nadav Peleg[2,3]

[1]Institute of Geography and Sustainability, University of Lausanne, Lausanne, Switzerland
[2]Institute of Earth Surface Dynamics, University of Lausanne, Lausanne, Switzerland
[3]Expertise Center for Climate Extremes, University of Lausanne, Lausanne, Switzerland
[4]Mountain Research Initiative, c/o University of Bern, Switzerland
[5]Center for Hydrogeology and Geothermics (CHYN), University of Neuchatel, Switzerland

Correspondence: Judith Eeckman ju.eeckman@gmail.com, judith.eeckman@unil.ch

Abstract. To gain a deeper understanding of the dynamics of the contribution of snowmelt to mountainous water cycles, it is necessary to better understand the processes controlling the infiltration of snowmelt into mountainous soils. This research uniquely combines snowmelt rate data with soil moisture dynamics, providing a comprehensive, three-year dataset. The integration of multiple measurement techniques and the estimation of the snowmelt rate through the measurement of snow resistivity offer a new perspective on snowmelt infiltration processes. The study area is located in Vallon de Nant, Swiss Alps. Measurement points are distributed in mid to high elevations in various alpine environments. Besides demonstrating the instrumental setup, we also investigated the snowmelt-infiltration dynamics in the study area. Results indicate that, although melt rates are considerably lower than soil saturated hydraulic conductivity values, the response times of shallow soil moisture and stream discharge to melt events are fast (from 2 to 5 hours). At the point measurement locations, snowmelt hardly infiltrates below 30 cm. These findings highlight how the fast recession of soil moisture peaks to snowmelt may limit the capacity of mountain soils to retain water, potentially increasing their vulnerability to dry periods in the future.

1 Introduction

Understanding the processes controlling the snowmelt infiltration in alpine soils remains one of the challenging questions in mountain hydrology. Due to steep slopes and erosion processes, alpine soils are generally relatively thin and commonly present textures from sand to silt (Legros, 1992). Infiltration processes in mountainous soils are controlled by two competing factors: (i) the coarse granulometry of superficial soils, which enhances their infiltration capacity (Legros, 1992); and (ii) the typically steep slopes, which increase the velocity of lateral transfer (Webb et al., 2018b; Carey and Woo, 2001). Kampf et al. (2015) provide an overview of the different snowmelt infiltration processes encountered in various mountainous areas. Evidence of fast lateral transfer in shallow soils during snowmelt periods is mentioned in several studies (Santos et al., 2018; Fang et al., 2019; Heidbüchel et al., 2012). Young waters (i.e., from snowmelt and superficial storage) have been shown to actively contribute to discharge during both winter and spring melt periods (Ceperley et al., 2020). An "inverse storage effect" (i.e., emptying of the most superficial soil layers) has been observed during snow accumulation periods (Benettin et al., 2017; Wilusz et al., 2020).

On the other hand, evidence exists regarding circulations in deeper layers, particularly through unconsolidated moraine deposits and fractured bedrock, observed in mountainous catchments during snowmelt periods (Schaefli et al., 2014; Meeks et al., 2017; Thornton et al., 2018; Carroll et al., 2019; Lorenzi et al., 2024). The question of the partitioning of meltwater fluxes into lateral transfers or deeper vertical infiltration therefore remains open, as do the preferential conditions for each of these processes.

One common method for assessing the contribution of soil water to discharge is natural tracer analysis, in particular stable water isotopes (Klaus and McDonnell, 2013; Beria et al., 2018; Michelon et al., 2022). However, transfers into superficial soils are hard to track via natural tracers because their signature is inconclusive. Other studies on this topic have deployed instrumental networks of soil moisture measurement probes. However, few studies couple these moisture probes with accurate estimations of the snowmelt rate. Current understanding of the physical processes involved remains insufficient to explain the role of the unsaturated zone in the infiltration of snowmelt in mountains. In particular, additional descriptions are needed of (i) the partitioning between surface runoff and vertical infiltration of snowmelt rate into soil layers, (ii) the depths reached by vertical percolation and the depth of preferential circulations for lateral transmission along the slopes, and (iii) the response times to melt events of both the soil moisture and the river discharge.

In addition, estimation methods of snowmelt rates, whether by modeling or by in situ measurements, are associated with high uncertainties. Despite a wide range of model formalisms, from simple temperature index methods to full energy balance methods, being applied to simulate the flux at the interface between snowpack and soil (Martinec, 1975; Rulin et al., 2008; Vionnet et al., 2011; He et al., 2014; Zhang et al., 2015; Thornton et al., 2021), modeling approaches still face large uncertainties in accurately representing snowmelt infiltration into soils. This is mainly due to large heterogeneity in soil and snowpack properties and a lack of measurements for these particular variables in mountainous areas (Meeks et al., 2017). Some studies apply direct monitoring of meltwater using snow lysimeters, ranging from simple buried rain gauges to complex melted water collecting systems (Kattelmann, 2000; Webb et al., 2018a). Other studies estimate the melt rate through the measured or modelled variation of snow depth or snow water equivalent (S_{WE}) of the snowpack (Kampf et al., 2015; Fang et al., 2019;

Archer and Stewart, 1995). However, these variables neither take into account the vertical heterogeneity of the snowpack nor surface effects such as sublimation or wind depletion. In addition, in situ melt measurement methods are often qualitative or have low temporal resolution, leading to inaccurate estimations of the response time of both soil water and river discharge to melt events.

This work aims to address the two issues of (i) providing a measurement framework for the estimation of snowmelt rate and (ii) accurately detailing the physical processes involved in the unsaturated zone during the infiltration of snowmelt at a study point. This paper proposes a method that enables the precise estimation over three years at an hourly resolution of both melting and infiltration processes. Three instrumental methods to estimate snowmelt rates are compared in order to provide a more robust quantification of this variable. The soil analysis methods are also described, including vertical conductivity estimation. Snowmelt infiltration into soil layers is monitored at depths up to 30 cm using a network of capacitive probes. These probes are deployed at the same locations where snowmelt is monitored, allowing for the tracking of the vertical penetration of melt flux into soil layers and accounting for spatial variations. We performed different analyses to (i) a multi-instrumental quantification of the snowmelt rate; (ii) a description of the processes controlling the partition between surface runoff and vertical infiltration during melt events; and (iii) a quantification of the vertical percolation of the melt flux and its lateral transfers along the slopes toward the outlet, including an estimation of response times.

The proposed multi-instrumental monitoring setup provides valuable insights into snowmelt infiltration dynamics in mountainous catchments. We present an implementation of our monitoring approach in Vallon de Nant. The monitoring was performed for three consecutive years (2021 to 2024), and winter field campaigns were conducted to provide validation measurements of snow properties.

2 Study area

2.1 Site description

The study area is located in Vallon de Nant (46.23°N, 7.07°E), a Swiss pre-Alpine catchment that contains typical alpine ecosystems, from deciduous forest to post-glacial recolonization (Fig. 1). The catchment area is 13.4 km^2 and the altitudes range from 1,200 to 3,051 m above sea level (a.s.l). The catchment is selected because of its importance for ecological monitoring and the quantity and duration of measurements available from decades of monitoring. Perret and Martin (2015) presented a detailed map of surface geomorphological units. Three main geomorphological units are described (Fig. 1B): (i) limestone cliffs from the Nappe de Morcles on the east ridge of the valley; (ii) active and passive moraine deposits from the Martinet glacial on the upper part of the valley; and (iii) flysch cliffs and associated screes and rockfalls on the west ridge of the valley. The majority of the superficial soils in Vallon de Nant are developed on top of ancient moraine deposits, screens, and landslides, resulting in sandy to silty, relatively shallow soils (Grand et al., 2016). While these formations are common in alpine areas, in this valley the accumulation of erosion material from the schist cliffs into small depressions has led to the development of unusually thick soils in places. Several studies have investigated the catchment's surface and subsurface hydrology (Antoniazza, 2023; Michelon et al., 2023; Thornton et al., 2022). Besides assessing the recent shift in snowmelt peak and its impact on the
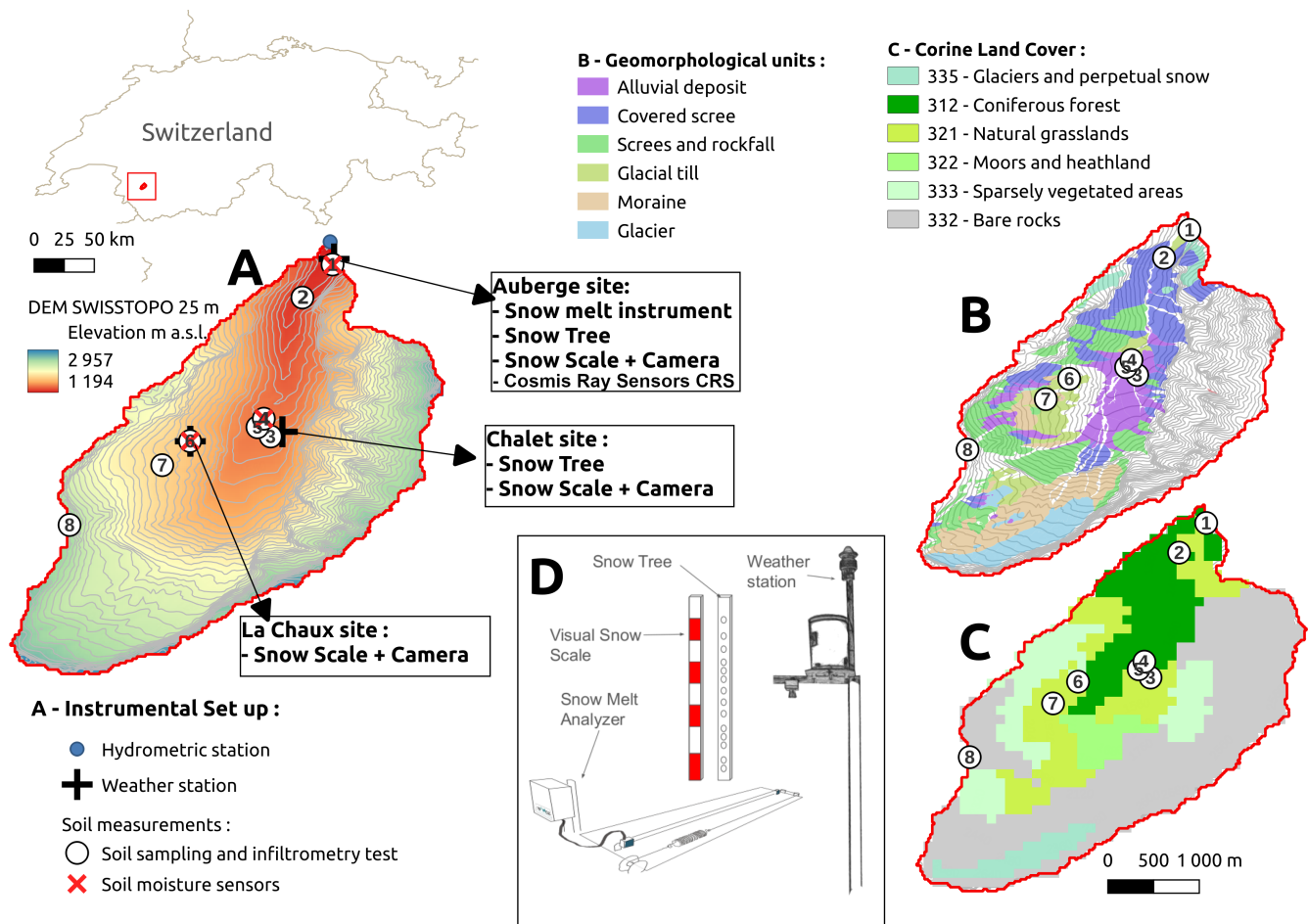
Figure 1. Vallon de Nant, Bex, Switzerland, and the locations of the instrument set up deployed in this study (A), together with (B) geomorphological units described by (Perret and Martin, 2015) and (C) Corine Land Cover 2006 (Aune-Lundberg and Strand, 2010). (D) is an illustration of the devices installed at the Auberge station for snowmelt monitoring : the snowmelt Analyzer (SMA), the Snow Tree and a weather station. The point numbers correspond to sample points in Table 1.

discharge, these studies showed that a limited understanding of snowmelt flowpaths hinders hydrological model development
80   for this catchment, which further motivated our research in this area.

2.2   Meteorological and hydrological data

A hydrometric station is located at the outlet of the catchment (Fig. 1A), recording hourly water levels since 2010. A rating curve has been computed based on 55 reference gauging performed at various water levels (Antoniazza, 2023). Moreover, weather data from three weather stations at different locations (at the elevations 1253 m a.s.l., 1485 m a.s.l. and 1780 m a.s.l.,
85   respectively) in the catchment is available since 2010 (Fig. 1A). These stations record total precipitation, near-surface air tem-

perature, atmospheric pressure, shortwave solar radiation, and wind direction and velocity at 5 minutes intervals, which were subsequently averaged to hourly timesteps. However, considering the exposure of these stations to harsh climatic conditions and their difficult access, the reliability of the recorded data is low and the time series presents many gaps. Moreover, as the climate stations are not heated, solid precipitation records are considerably underestimated (Benoit et al., 2018; Thornton et al., 2021). Consequently, the estimation of precipitation in the catchment remains highly uncertain. Precipitation uncertainties were not quantified as this is not the main focus of this work, and this limitation is presented in the Discussion section.

Daily remote sensed information on Snow Cover Area (SCA) is available at the 500 m resolution from the MODISA1 Level3 remote product (Hall et al., 2009). We used this product to describe the overall dynamics of the snow cover at the catchment scale. However, its spatial and temporal resolutions are not sufficient to compare this product at the pixel scale to the in-situ snow measurements.

3   Monitoring and data collection

Three different types of monitoring devices were deployed to obtain local values of snow depth, extent of snow cover, snow water equivalent (S_{WE}), and snowmelt rate.

3.1   Snowmelt Analyzer

The SnowMelt Analyzer (SMA) is a unique system for automatic and continuous measurements of diverse snowpack parameters developed by SOMMER Messtechnik. This monitoring device has been used in various studies in alpine environments (Sommertechnik, 2009), and can be used independently or in combination with a more complete instrumental setup for snowpack analysis. Here, the configuration of the instrument that allows the measurement of the liquid and solid water content and density of the bottom snow layer is chosen. The assumption made in this approach is that the liquid water content of the bottom snow layer (Λ, lowermost 7 cm) can be used as a proxy for the snowmelt rate. Snowmelt rates are derived from the direct measurement of the liquid water content of the snowpack through snow electric resistivity. The instrumental method has previously been shown to yield reliable assessments of snowmelt rates in various alpine studies (French and Binley, 2004; Gance et al., 2016; Bloem et al., 2020).

The SMA instrument consists of a metal frame set up in a suitable position on level ground (Fig. 1D). A weather and UV-resistant sensor band penetrates the snow and measures the volumes of ice, water, and air content in the snowpack using the variation of impedance between two connected electrodes. Three aspects were considered in choosing the device location: (i) installing the SMA on flat ground with snow conditions representative of the area and orienting the frame to avoid wind effects; (ii) selecting soils with significant storage and infiltration capacity, specifically deep alpine meadow soils; and (iii) ensuring ease of access and power supply. Consequently, the SMA was deployed near the Auberge climate station at 1253 m a.s.l (Fig. 1A). This mid-altitude location, with its developed soil, allows for the analysis of snowmelt rate and represents a favorable case for snowmelt infiltration compared to typical alpine sites with finer soils and steeper slopes.

3.2 SnowTree and visual scale

To estimate the snow cover extent in the surroundings of the measurement points, three visual scales coupled with time-lapse cameras were installed in the vicinity of the three climate stations (Fig. 1A). The images obtained from the cameras were evaluated in two respects: (i) the graduation reached on the visual scale, which gave the local snow depth with a 10 cm accuracy; and (ii) the qualitative extent of snow cover over the visible landscape, divided into three categories: *no snow*, *partially covered surface*, and *covered surface*. Despite the limited nature of such data, they provide valuable information about snow conditions during the measurement periods.

In addition, to locally assess the snow depth, two "SnowTree" instruments were developed and deployed at the Auberge and Chalet measurement points (Fig. 1A). The SnowTree is a 2.5 m high wooden mast, equipped with small *iButton* thermometers, which provide good performance for many environmental science applications (Hubbart et al., 2005), glued at 5 or 10 cm intervals. Temperatures were recorded every two hours. This instrument aims to track the snow depth by discriminating between thermometers covered by snow or not covered, with a ±5 cm accuracy. This instrument complements the observations made with the visual scale, with a vertical accuracy of ± 20 cm. In addition, this instrument is simpler to install than an optical snow depth sensor, because it does not require any structure or power supply, which is crucial for operations in remote mountain environments. Reusser and Zehe (2011) propose using the standard deviation of the hourly temperatures computed over 24 hours (σ) for this differentiation, as the diurnal amplitude of temperatures is lowered when a sensor is covered by snow. It appears during the study that the SnowTree better monitored the snow depth when it was well exposed to direct solar radiation, i.e., after mid-January (time-lapse images showed undetected frosted residual snow remaining along the wood mast). Indeed, in a narrow and shadowed valley like Vallon de Nant, the diurnal heating due to solar radiation when the sun position is low in winter is not dramatically varying and the determination of snow depth based on logger temperature is challenging. This issue is tackled by applying different thresholds whether the daily temperature exceeds $1°C$:

$$
\begin{cases}
\text{snow,} & \text{if } T_{day} < 1°C \text{ and } \sigma < 4.5 \\
\text{snow,} & \text{if } T_{day} > 1°C \text{ and } \sigma < 1.4 \\
\text{no snow,} & \text{otherwise,}
\end{cases}
\tag{1}
$$

where T_{day} [°C] is the average daily temperature and σ [°C] is the standard deviation of the hourly temperatures computed for each day.

Values of σ from 0.5°C to 5°C with step of 0.1°C have been tested for each of these two thresholds. The optimal value retained for each threshold minimizes the average RMSE criteria, using the daily snow height observed at the visual scale as reference time series. This optimization step is performed separately for days with $T_{day} < 1°C$ and $T_{day} > 1°C$. No multi-parameter optimization is performed.

This differentiated empirical threshold, combined with manual checking of the images from the camera, makes SnowTree a potentially valuable instrument for assessing snow depth in remote areas. The two SnowTrees and the visual scales were installed between November 2022 and March 2023 (2022-2023 winter) but were not maintained for the 2023–2024 winter

due to lack of manpower. Instead, a classical optical infra-red snow depth sensor was installed at the Auberge meteorological station in November 2023, which recorded hourly data.

3.3 Cosmic Ray Sensor

Hydroinnova's Cosmic Ray Sensor (CRS) monitoring device was installed at the Auberge station to measure snow water equivalent (S_{WE}) over a uniquely large footprint (Fig. 1). The advantages of the device, beyond the large footprint, are that it is automatic, easy to install, and requires little maintenance. The basis of the technique is that hydrogen contained in the snowpack attenuate downward neutrons coming from cosmic rays. The amount of attenuation is directly related to the mass of intervening snow, and by extension the amount of S_{WE}. The method described by Desilets (2017) to convert incoming neutrons count into S_{WE} value was used:

$$S_{WE} = -\Lambda \ln \frac{N}{N_0}, \tag{2}$$

and

$$N = f_{sol} N_{raw} \exp\left[(P - P_0)\beta\right], \tag{3}$$

where N_{raw} [count h^{-1}] is the measured incoming neutrons count, P [hPa] is the atmospheric pressure, P_0 [hPa] is the reference barometric pressure and N_0 [count h^{-1}] is the proton flux in the absence of snow. Λ [-] and β [-] are fixed parameters, following the technical recommendations (KIT, 2015). To complement these S_{WE} time series, local density measurements were carried out during the winter of 2022–2023 near the Auberge station, using the method of weighing cylindrical samples: snow profiles were dug, snow samples were collected horizontally with a metal cylinder of volume 550 cm^3 (diameter 12 cm). The collected snow is weighed to calculate the density of the snow sample. At each location, a sample is collected approximately 7 cm from the ground (which corresponds to the SMA measurement height) and, if the depth of the snowpack allows, another sample is taken in the middle of the vertical.

3.4 Soil sampling and analysis

To describe the variety of soils in the study area, eight varied sampling sites were chosen. The physiographic characteristics of these eight sites and the instrumental set up are presented on Table 1 and the point ID are referenced on Fig. 1. At each site, soil cores were taken and the granulometry of the sampled soil were analysed. Infiltrometer tests have been conducted for seven of the eight sampling sites (expect the Bastion point for technical reasons at this distant point). Soil moisture probes have been installed at three of these eight sampling sites that are located close to the climatic stations: the Auberge, Petit Pont and La Chaux points (see Table 1). The locations are chosen to represent the different geomorphological characteristics and environments in the catchment, from deep soil covered by mixed forest to shallow soils developed above the moraine deposit. Both grazed and non-grazed sites were sampled. In particular, four points at different elevations (Auberge, Petit Pont and La Chaux) were specially analysed because they present particularly deep soils, resulting from the accumulation of material eroded from the schist cliffs on the western side of the valley. Evidence of superficial water saturation in springs observed at

Table 1. Physiographic characteristics of the nine soil sampling points: location, soil depth, geomorphology (Perret and Martin, 2015) and CLC2006 Land Cover (Aune-Lundberg and Strand, 2010) classifications, together with the estimation of soil parameters: granulometry, water content of the total soil column at saturation w_{sat} and at the wilting point w_{wilt}, field capacity w_{fc} and hydraulic conductivity at saturation K_{sat}. AD - Alluvial deposit; GT - Glacial till; SR - Screes and rockfall; CF - Coniferous forest; NG - Natural grasslands; BR - Bare rock.

	Auberge	Pissenlit	Chalet	Petit Pont	Protegée	LaChaux	Combe	Bastion
Point ID	1	2	3	4	5	6	7	8
Physiographic characteristics								
Lat/Lon [°N/°E]	46.251/7.110	46.247/7.106	46.229/7.102	46.231/7.102	46.230/7.101	46.229/7.092	46.225/7.088	46.218/7.077
Elevation [m.a.s.l.]	1257	1281	1491	1473	1479	1777	1853	2497
Soil depth [cm]	69	40	32	>130	10	>130	90	65
Geomorphology	AD	AD	AD	AD	AD	GT	GT	SR
CLC2006	CF	CF	NG	NG	NG	NG	NG	BR
Pasture	No	Yes	Yes	Yes	No	Yes	No	No
Instrumental devices								
Climatic station	✓	-	✓	-	-	✓	-	-
SnowTree and visual scale	✓	-	✓	-	-	-	-	-
5TM sensor depth [cm]	5, 10, 20, 30	-	-	25	-	25	-	-
Infiltrometry tested	✓	✓	✓	✓	✓	✓	✓	-
Estimation of soil parameters								
Clay [min:max] [%]	14.9 [13.5:15.8]	17.3 [14.7:19.8]	14.1 [13.1:15.2]	15.5 [10.4:19.1]	9.1 [6.3:11.9]	13.1 [10.5:16.1]	15.15 [12.9:17.4]	16.2 [15.0:18.1]
Silt [min:max] [%]	60.5 [56.2:61.9]	70.9 [69.3:72.7]	70.2 [66.8:72.8]	67.3 [50.6:72.8]	51.9 [42.2:61.6]	62.7 [58.0:65.8]	62.1 [57.6:64.4]	63.2 [61.5:65.3]
Sand [min:max] [%]	24.6 [22.4:30.3]	11.7 [10.9:12.6]	15.7 [12.0:20.2]	17.2 [10.4:39.0]	38.9 [26.5:51.4]	24.2 [19.9:31.5]	22.9 [19.1:29.5]	20.5 [16.6:23.0]
w_{sat} [m^3 m^{-3}]	0.468	0.482	0.477	0.476	0.452	0.468	0.47	0.472
w_{wilt} [m^3 m^{-3}]	0.143	0.154	0.139	0.146	0.11	0.134	0.144	0.149
w_{fc} [m^3 m^{-3}]	0.229	0.24	0.225	0.231	0.19	0.218	0.229	0.2
K_{sat} [mm h^{-1}]	252.2	79.2	59.1	97.7	127.7	20.2	185.4	-

these sites for the three years studied motivates the detailed analysis of the dynamics of their contribution to the hydrological system. 5TM/DECAGON capacitive sensors were used to measure soil moisture and soil temperature at hourly intervals at different depths at these three points (Fig. 1). These sensors were installed in August 2021.

3.5 Granulometry analysis and pedotransfer functions

Vertical descriptions of the soils and sampling were performed at one or two auger holes for each sampling point. Granulometry analysis was then performed for each of the samples collected for the main observed horizons at the eight sampling points. Particle size distributions were determined via laser granulometry analysis (Blott et al., 2004). The empirical pedotransfer functions proposed by Clapp and Hornberger (1978) were used to compute values of soil water content at saturation (w_{sat} [m^3 m^{-3}]), wilting point (w_{wilt} [m^3 m^{-3}]), and field capacity (w_{fc} [m^3 m^{-3}]) from the clay C [-] and sand S [-] fraction of each sample:

$$w_{sat} = (-1.08S + 494.305) \cdot 10^{-3}, \tag{4}$$

$$w_{wilt} = 37.1342 \cdot 10^{-3} C^{0.5}, \tag{5}$$

and,

$$w_{fc} = 89.0497 \cdot 10^{-3} C^{0.3495}. \tag{6}$$

The soil parameters were computed for each depth and then averaged on the soil vertically to get one value for each of the 9

195   sampling points. To consider commensurate variables, the relative water content W_r [-], was used for each soil layer:

$$W_r = \frac{W - w_{wilt}}{w_{sat} - w_{wilt}}, \tag{7}$$

where W [m^3 m^{-3}] is the measured soil water content. A W_r equal to 1 means that the saturation of the soil layer is reached, while 0 means that its wilting point is reached.

    The clay, sand, and silt fractions resulting from the laser granulometry analysis, together with the water content at different

200   phases computed through the Clapp and Hornberger's equation, are summarized in Table 1. Using the USDA soil texture classification, all the samples are in the Silty Loam category, which is consistent with silty moraine deposits. In addition, the results are consistent with previous studies in Vallon de Nant (Grand et al., 2016; Cianfrani et al., 2019). The hydraulic conductivity at saturation (K_{sat}) and the average soil water content are also presented in Table 1. The values of K_{sat} obtained are consistent with general values considered by Cosby et al. (1984) for soil classes. Cattle trampling and grazing affect

205   K_{sat}; non-grazed locations (Combe, Protegee, Auberge) present K_{sat} values that are considerably higher than those at grazed locations (Chalet, LaChaux, Pissenlit). In addition, a dense grass root system is observed in Combe, which might act to reduce the infiltration rate at this location.

3.6   Infiltrometry test

The Beerkan infiltration method was used to determine the saturated hydraulic conductivity at the sampling points. This method

210   is detailed by Haverkamp et al. (1994) and Braud et al. (2005). A PVC cylinder of diameter 25 cm was used with 1 L of water poured at each iteration. For estimating retention curves and hydraulic conductivities, the BEST (Beerkan Estimation of Soil Transfer parameters) method (Lassabatère et al., 2006) was applied. BEST is approaching the series of cumulative infiltration rates and instantaneous infiltration rates by the expressions provided by Haverkamp et al. (1994), which involves the sorptivity and the hydraulic conductivity at saturation K_{sat} of the soil (Van Genuchten, 1980; Burdine, 1953; Brooks and Corey, 1966).

215   These expressions involve three parameters of form which are determined from particle size distributions (Fuentes et al., 2017) and based on capillarity models (Haverkamp et al., 1994).
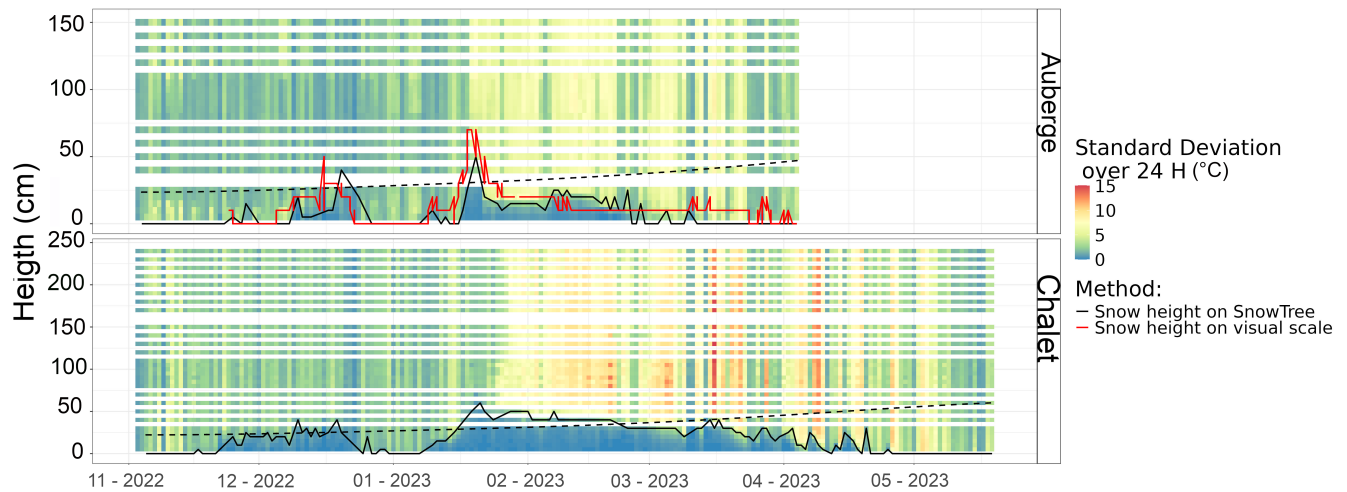
Figure 2. Temperature standard deviation computed over 24 h recorded by the iButton loggers on the SnowTree instrument at the Auberge and Chalet locations (background colors). Black and red solid lines represent the snow depths obtained from the SnowTrees and the visual scales, respectively. The dashed line corresponds to the intensity of solar illumination received at the measurement points. The solar illumination in the valley, including hill-shading effects is computed with the *hillshading* function (*insol* R package; Corripio and Corripio, 2019).

4 Results

4.1 Multi-instrumental assessment of snowmelt

At the Auberge station, the dynamics of the snow depths deduced from the Snow-Tree measurements are consistent with the observation at the visual scale (Fig. 2). In particular, the snow depth peak on 21 January 2023 is represented with the same timing in the SnowTree and the visual scale results. In addition, the only point snow density measurement taken within the CRS recording period (recorded on 5 December, 2022) gave a snow density of $\rho_{obs} = 293 kg.m^{-3}$ and a 24 cm snow depth. For this time point, the CRS provided a S_{WE} of 7.9 cm, which is equivalent to 26.9 cm using the ρ_{obs} density. This shows that the estimation of S_{WE} by the CRS led to an estimation of snow depth consistent with the snow depth estimated at the Auberge Snow-Tree (26.9 cm against observation of 24 cm). These measurements reinforces the robustness of the Snow-Tree results.

The two SnowTree instruments at the Auberge and Chalet site allow to estimate the seasonal dynamics of snow depths. Over the monitored winter (2022-2023), the average snow depth at Auberge is 16 cm and 27 cm at Chalet. The dynamics at the two sites are consistent, with the beginning of the snow accumulation in mid-November (Nov 25 at Auberge and Nov 17 at Chalet), and the disappearance of the snow cover between late December and mid-January. The snow peak on 21 January is observed at the two sites.

Figure 3, despite the time series being short (the CRS instrument stopped due to an unstable electric feeding in early February 2023), the S_{WE} measured by the CRS and the liquid water content of the bottom layer measured by the SMA (Λ) can be compared at the hourly time-step. The recorded period consists of two periods: i) between 21 December and 15 January,
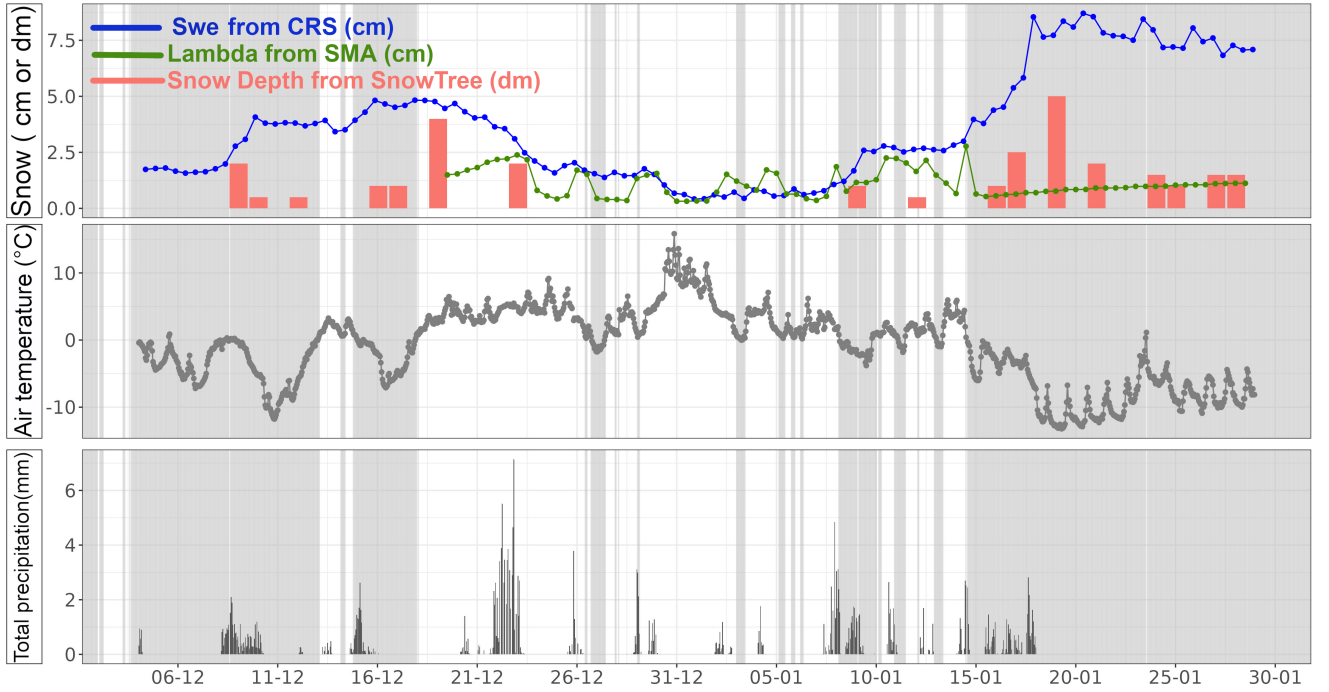
Figure 3. Snow Water Equivalent computed from Cosmic Ray Sensor measurements S_{WE} [mm], together with the liquid water content of the bottom snow layer measured by the SnowMelt Analyzer Λ [%]. The grey bands indicate the time step with temperatures below $1^\circ C$.

a period with high temperature (above $1^\circ C$) and liquid precipitation happening and ii) between Jan, 15th and Jan, 20th, a period without precipitation and with temperature below $1^\circ C$. During the first period, Λ appears to actively react to liquid precipitation, which is consistent with a rapid transfer of liquid water through the snow pack. On the opposite, during the second period, the S_{WE} reacts to the changes in temperature, whereas Λ remains stable. This corresponds to a compaction of the snow pack not associated with melt.

This shows that the variation of S_{WE} does not necessarily correctly represent the melt rate, as it is often assumed in other studies (Kampf et al., 2015; Fang et al., 2019; Archer and Stewart, 1995). By focusing on the lowermost snow layer, our approach isolates actual melt from other transformations of the snow pack such as icing, compaction or wind depletion, allowing for more accurate estimations of local melt rates – a key target variable. However, Λ values must be considered with caution when liquid rainfall happens (see section 5).

4.2 Infiltration/runoff partition

The partition between surface runoff and infiltration can occur either by exceeding sthe water content at saturation (w_{sat}) of the first soil layer (Dunne runoff) or by exceeding the soil conductivity at saturation (K_{sat}) (Hortonian runoff). At the Auberge site, or the entire monitored period (22'287 hours), snowmelt is detected during 2'086 hours, i.e. 9.3% of the time. Among these

time steps with melt occurring, the first soil layer reached saturation for 326 hours (15% of the hours with snowmelt). This shows that snowmelt resulted to Dunne surface runoff in 15% of the melt event at the Auberge site during the monitored period.

Regarding Hortonian runoff, based on the obtained K_{sat} value for the Pissenlit site (see Table 1), $DeltaLambda$ exceeded K_{sat} for 91 hours during the recorded period (4.3% of the hours with snowmelt). Both conditions with $DeltaLambda$ greater than K_{sat} on a saturated soil happened for only 13 time steps during the monitored period. Depending on the site, Hortonian runoff can occur for between 4.3% (at Auberge site) and 100% (La Chaux site) of the melt events.

Figure 4 shows that snowmelt produces surface runoff mainly during early winter and spring seasons, with low $DeltaLambda$ during February and March. However, the runoff processes vary strongly between winter and spring season. During spring (Figure 5a), the peaks of snowmelt that exceed K_{sat} are mainly associated with changes in the energy budget, led by diurnal variations of radiation and temperature. The runoff generation results from $DeltaLambda$ greater than K_{sat} around the maximal peak of diurnal temperature. The response of the soil layers, as well as the river discharge is between 3 hours and 5 hours (graphical assessment). The dynamics for early winter melt is less clear (Figure 5b): both Dunne and Hortonian runoff occurred but the response of neither the soil layers nor the river discharge to melt event is clear. The delay induced by soil storage during early winter melt strongly varies between the events.

4.3 Lateral transfer of melt flux

Figure 4 and Figure 5 show that during both the spring and the winter melt, the response of the soil layer at 30 cm depth is limited. This means that the infiltration of snowmelt hardly exceeds 30 cm at this measurement point. The main increase of the soil water content of this soil layer mainly coincides with liquid precipitation in late spring. This observation suggest that, despite melt flux can infiltrate in the superficial soil layers when neither K_{sat} nor w_{sat} are exceeded, deeper infiltration does not occur at the Auberge site. These results suggest that lateral transfer in superficial soil layers (above 30 cm depth) dominates the vertical infiltration in a mountainous context, even in a context favorable to infiltration such as the Auberge site. The first soil layers can then represent a zone where lateral transfers towards the outlet are significant. These results corroborate those of Ceperley et al. (2020), who found that young water is the main contributor to discharge during winter. Kampf et al. (2015) also noticed empirical evidence of lateral transfers during spring melt, based on audible sounds.

We explore the spatial variability of snowmelt-infiltration dynamics, focusing on the hydrological response at 25 cm depth at the Chalet, La Chaux and Auberge sites (Fig. 6). The annual dynamics of the soil moisture are similar at the three measurement points: overall soil moisture increases with increased snow pack. This is clearly visible in December 2022. A graphical assessment of the response times of the soil moisture shows that the peaks due to liquid to mixed precipitation in winter, as well as liquid precipitation in summer are shifted by only two hours between the three sites. The peaks of soil moisture due to diurnal melt in spring are shifted from about five hours between Chalet and Auberge stations. This is due to the lag between diurnal snowmelt at different altitudes, whereas precipitation happens more simultaneously in the catchment. One can also note that the soil moisture peaks are less pronounced at La Chaux, compared to the other two. This is due to the fact that the K_{sat} value measured at La Chaux is lower than at Chalet of Auberge, leading to more occurrences of surface runoff that infiltration at La Chaux site.

These time series show that, across the whole catchment, the reaction of soils to both snowmelt and liquid precipitation is fast (less than 6 hours) and happens almost simultaneously (with a shift of less than 5 hours). This demonstrates that the transfers along the catchment toward the outlet are fast, for liquid precipitation but also for snowmelt.

5 Discussion

5.1 Uncertainties in snowmelt estimation

Although this instrumental approach makes it possible to enhance the robustness of snowmelt measurement, significant uncertainties remain. In particular, rain-on-snow phenomena strongly disturb the measurements. In Figure 3, between 21 December and 15 January (period with liquid precipitation happening on snowpack), Λ values recorded by the SMA react to precipitation within the next hour. This raises the issue of the representativeness of the SMA measurement in such conditions, as well as the delay induced by vertical percolation of the liquid water through the snowpack. The transfer time of liquid water during rain-on-snow phenomena can be considered as the fastest transfer through the snowpack, i.e. the minimal delay induced. This means that the Λ time series might include a ± 1-hour uncertainty.

In addition, the main weakness of the SMA instrument is that very thin snowpacks of less than the sensor ribbon size (7 cm) are inaccurately represented. However, this situation has little impact in terms of hydrology as the equivalent volumes are low. Λ variations recorded with very thin snowpacks must therefore be considered with caution. Lastly, one can also note that the positive variations of Λ may also be due to refreezing of the bottom layer in the case of very thin snow cover. This is a limitation of the estimation of melt rate. However, since the SMA also provides the ice content of the bottom snow layer, refreezing periods can be determined.

5.2 Inter-annual variability and climate change

The three monitored winters markedly differ in terms of snowpack dynamics (Fig. 4). The winter 2021–2022 consisted of an intense melting period in early winter, the 2022–2023 winter presented intermittent snow conditions, with the alternation of accumulation and melting periods, and the 2023–2024 winter exhibited a shorter snow cover period but with a melt period concentrated in the spring season. For the 2021–2022 winter, the first snow accumulation period occurred in early winter (December), followed by a warmer melting period in January, another accumulation period in late winter (March), and a gradual melting in April. For the 2022–2023 winter, the snow season consisted mainly of an alternation of accumulation and fast melt periods due to the sharp increase in temperature. The spring melt period expanded from mid-February to the beginning of April. In Figure 7, the behavior of snowmelt, as well as Dunne runoff and Hortonian runoff, strongly differ between the three monitored winters. Consequently, this three-year dataset does not allow for describing the seasons of majority influence of the different types of runoff and infiltration processes during snowmelt.

The potential implications of these results in the context of climate change can be considered. The amount of solid precipitation is projected to decrease, and the onset of the melt is expected to commence earlier (Masson-Delmotte et al., 2021),

changing the snowmelt infiltration dynamics. In the Swiss Alps, for example, a reduction in snow amount, a shortening of the melt period, and faster melt rates associated with shortened snow events are expected (Fischer et al., 2022). The rapid infiltration in the upper soil layers and the fast response of the river flow highlighted in this work corroborate the increase in flood risk during the spring season (Kundzewicz et al., 2014), in particular in the context of increased melt flux intensities. In addition, the expected increases in the duration of the low-flow period (from July–August to June–August) could lead to an increasing risk of damage to riverine ecosystems (Pletterbauer et al., 2018) and could affect hydroelectrical production. This work emphasizes that the fast response of soils and discharge to snowmelt increases the risk of low flow and water shortage outside of the melt period. This highlights the dependency of water availability on the delayed melt of the snowpack at high elevations.

5.3 Spatial variability of soil-water processes

The eight points sampled for the soil analysis represent various soil contexts. Some sites present low values of K_{sat}, such as the LaChaux and Chalet sites. The impact of pasturing on the K_{sat} values for nearby sites can be noted, just like between the Auberge and Pissenlit sites and between the Combe and LaChaux sites. For these four sites, cow pasture significantly reduces the soil conductivity at saturation.

Other sites present higher K_{sat} values, like the Protegee (protected from cows) and La Combe sites. This variability illustrates that some areas may actually block the infiltration of meltwater and produce significant surface runoff. Conversely, Combe-like areas may act as recharge zones, with higher vertical infiltration rates. This emphasizes the crucial role of these areas in enabling infiltration in mountains. However, eight points remain limited for such a heterogeneous environment, and the representativeness of these sites is necessarily restricted.

In addition, the response of deeper soils and groundwater is not considered here. In particular, the flows and storage in unconsolidated subsoils, such as moraine deposits from landslides and rockfalls, can be significant, especially in the alluvial fan which is present in the middle of the valley. This work paves the way for a better understanding of the contribution of snowmelt to deep water recharge in mountainous regions: at the study site, the superficial soil layers (i.e., above 30 cm) appear to limit the infiltration flux toward deeper zones. The assumption can then be made that the recharge of deep storage might preferentially occur in specific areas presenting little or no developed soils, such as bare rock or uncovered moraines. This assumption could be explored using advanced modelling approaches (Thornton, 2020). Further instrumental work could allow for a better description of the circulation below 30 cm depth. Interactions between the fast-reacting unsaturated zone of the soil and the snow-groundwater system at the catchment scale could then be considered in future work.
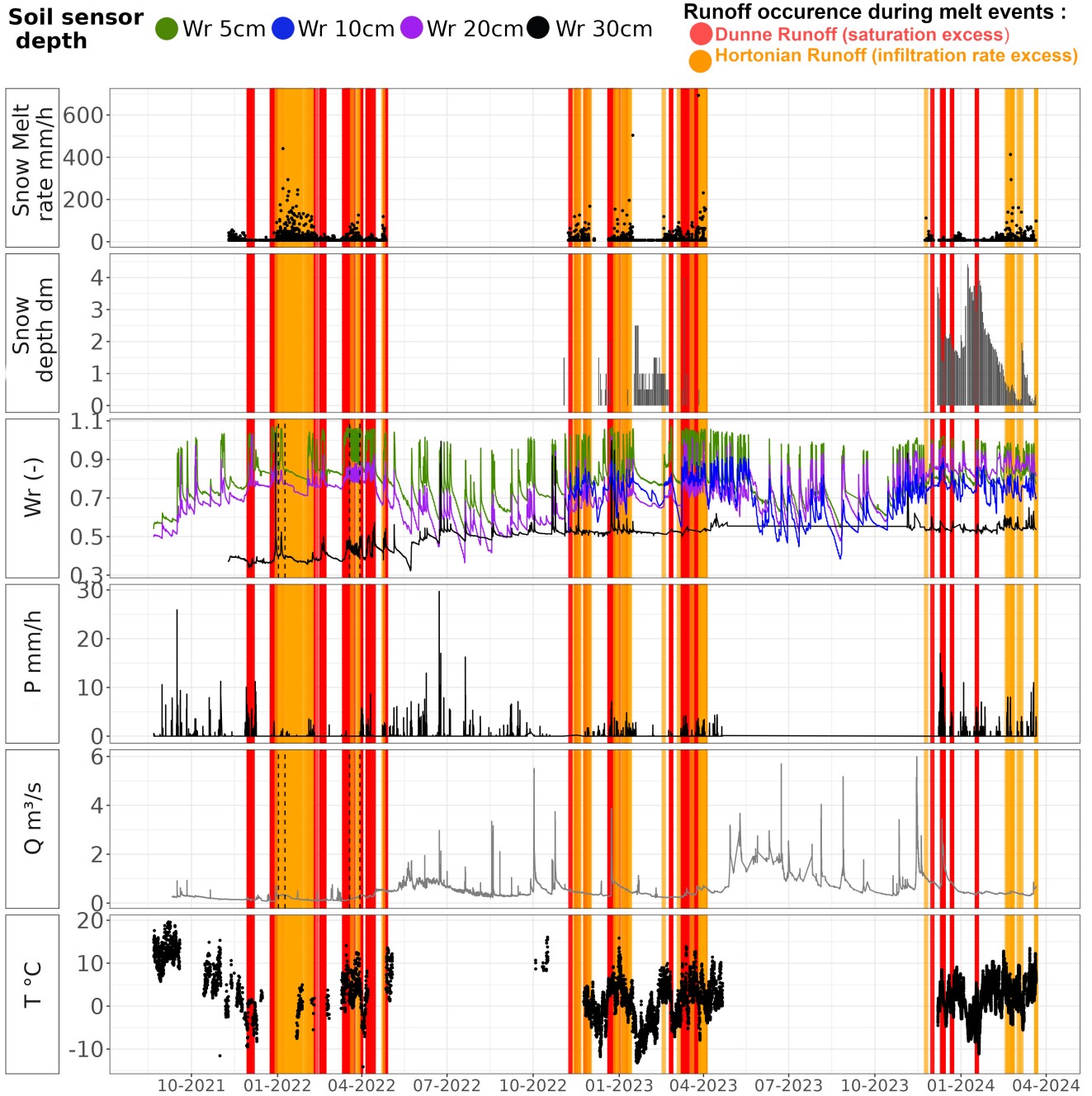
Figure 4. Soil moisture (W_r), Precipitation (P), Temperature, discharge at the outlet (Q), Water content of the bottom snow layer and snow depth measured at the Auberge point, together with K_{sat} values and zoom into periods of interest, for the entire recording period: from September 2021 to March 2024. The vertical grey lines represent the time steps when the hourly melt rate overpasses the K_{sat} value measured at the Auberge soil sampling point.

(a) Example 1: Diurnal melt during Spring 2022
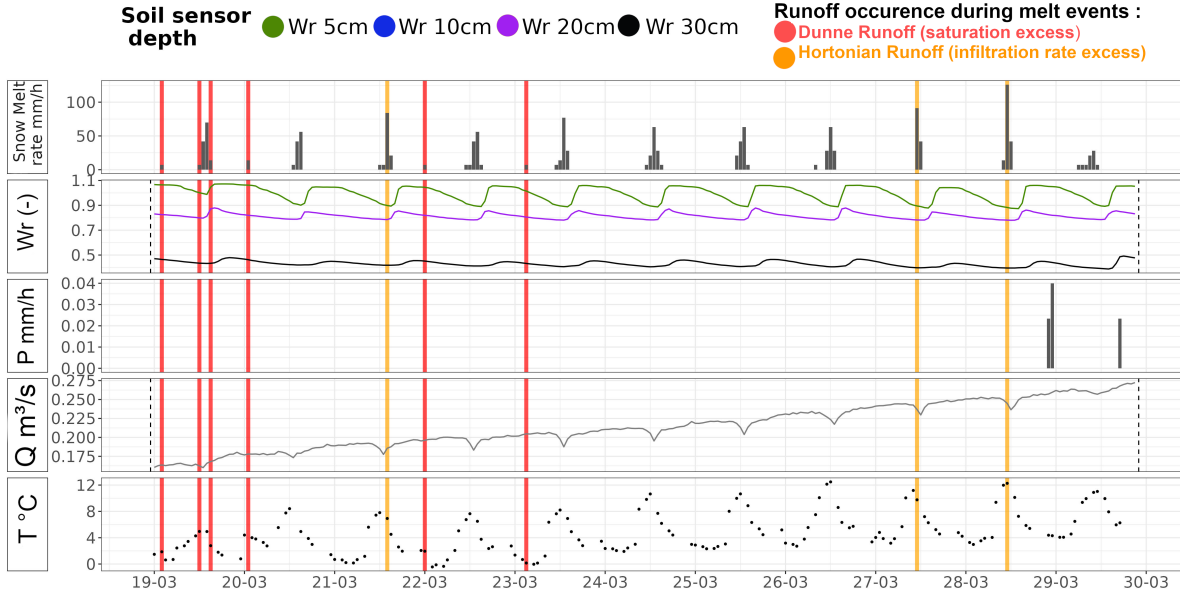
(b) Example 2: Early winter 2021
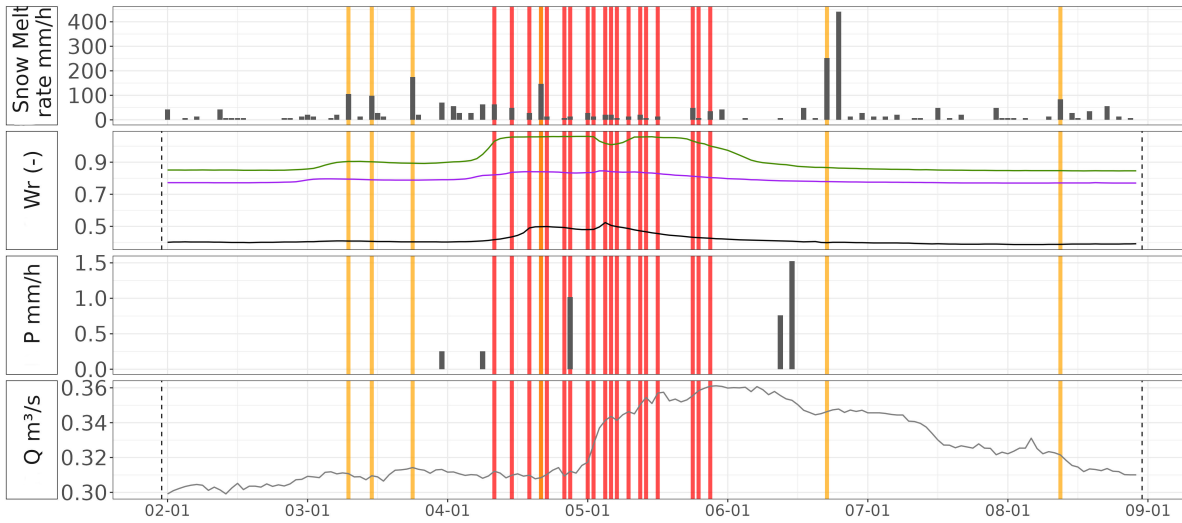
Figure 5. Zoom into specific periods for the variables Soil moisture (W_r), Precipitation (P), Temperature, discharge at the outlet (Q), Water content of the bottom snow layer and snow depth measured at the Auberge point.
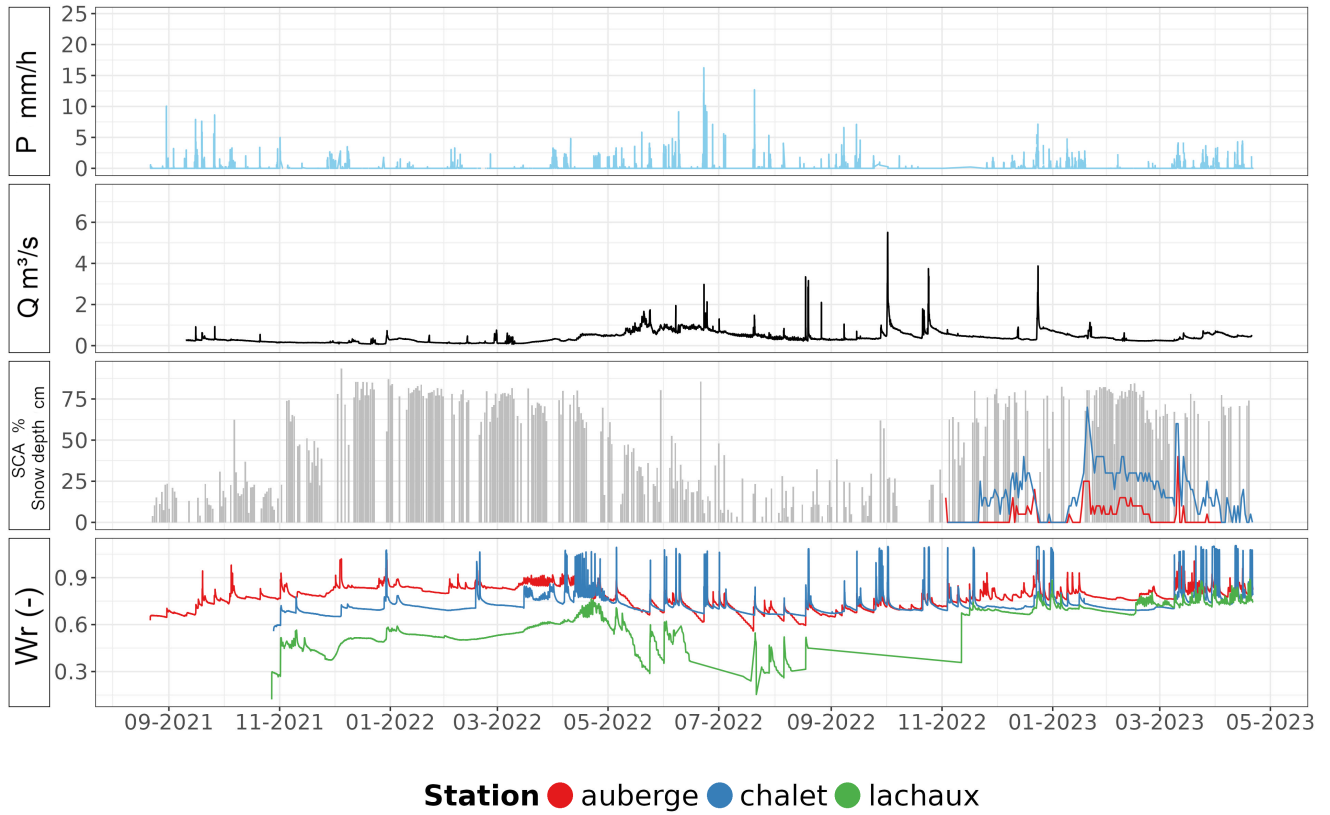
Figure 6. Soil moisture measured at 25 cm depth at the three measurement points, together with precipitation recorded at Auberge station, the MOD10A1 daily values of Snow Cover Area, on average over the entire catchment and the snow depths estimated at the SnowTree instruments at Auberge and Chalet spots.
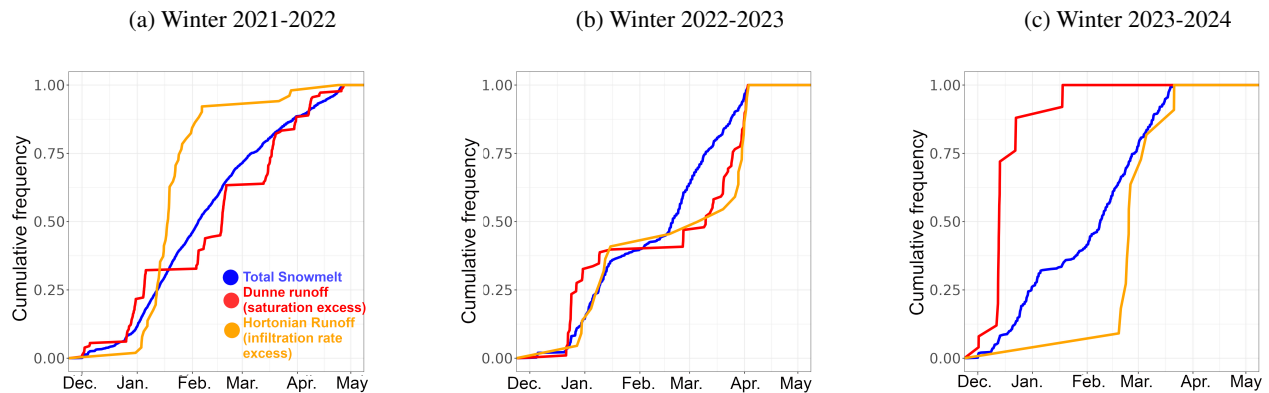
Figure 7. Cumulative frequency of occurrence during each of the three monitored winters, for snowmelt (blue), as well as Hortionian runoff (Orange) and Dunne runoff (Red) happening during melt events.

6 Conclusions

The results explore : (i) Comparing three different methods to estimate snowmelt rate at the local scale ; (ii) Comparing the intensities of melt rates with the infiltration capacity of soils to better quantify the partition between surface runoff and infiltration of the melt flux; and (iii) Describing the dynamics of vertical and lateral transfers of the flux issued from snowmelt in the superficial soil layers and the response of the stream discharge to melt events to better quantify the response of the catchment to melt events.

The main conclusions of this instrumental experiment are as follows:

1. Snow-Tree temperature measurements align well with visual observations, confirming their reliability. S_{WE} estimates from the CRS are consistent with snow depth measurements. The study shows that S_{WE} variations do not always reflect actual melt, as other snowpack processes (e.g., compaction) can interfere. Focusing on the bottom snow layer provides a more accurate melt rate estimation.

2. The measured snowmelt rate is generally lower than the soil conductivity at saturation, allowing infiltration of melt flux in the first soil layers. For the Auberge site, Hortonian runoff (exceeding soil conductivity) occurred during 4.3% of the melt events. Dunne runoff (due to soil saturation) happened in 15% of the melt events. The infiltration processes strongly differ between winter and spring. In spring, runoff is mainly driven by diurnal temperature variations, while winter runoff patterns are more irregular.

3. Soil layers below 30 cm are little influenced by snow melt, and soil moisture responses at the three monitored sites show rapid and simultaneous reactions to melt and precipitation (delay <5 hours), confirming fast water transfer across the catchment. No inter-seasonal storage in soils is observed.

Even though this work is limited by compiling only three years of data, which occasionally includes significant gaps and restricted recording periods, with limited measurement points and uncertainties, especially regarding weather and snow depth data, it nonetheless provides an uncommon combination of soil and snow data using various acquisition methods. The resulting dataset represents a valuable contribution to the understanding of mountainous environments. In addition to its contribution to process understanding, these snow-and-soil records can be used as validation or calibration data to improve process simulation in physically-based hydrological models, in particular for local scale studies. These observations could assist in refining aspects physically based surface schemes implemented at the measurement point.

Data availability. All the data produced in this work are freely available through the dedicated Zenodo platform: zenodo.org/communities/vdn/. Soil moisture, soil temperature data and granulometry results can be download at zenodo.org/records/10136586 (Eeckman, 2023). SMA snowmelt rate and snow water content data, as well as SnowTree data can be download at zenodo.org/records/11580271 ,(Eeckman, 2024).

370 *Author contributions.* JE initiated and developed the research project, raised funding for the instrumentation and fieldwork, carried out the fieldwork and data analysis, as well as the writing of the paper. NP advised the writing of the paper and significantly contributed to its redaction. BD actively assisted with the fieldwork and participated in the processing of field data. FM actively assisted with the fieldwork and preparation of materials. JT contributed to the analysis of CRS data and helped correcting the manuscript. PB: Funding acquisition and project management for JT, manuscript revision and correction.

375 *Competing interests.* NP is a member of the editorial board of Hydrology and Earth System Sciences.

Acknowledgements. The SMA and SnowTree instruments were financed thanks to the investment fund (FINV) of the University of Lausanne. The field assistance was financed thanks to the contribution of the UNIL Institute of Geography and Sustainability (IGD). Other costs related to fieldwork were financed by the IGD fund for fieldwork. The authors would like to thank the director of the IGD for this support. NP was supported by the Swiss National Science Foundation (SNSF), Grant 194649 ("Rainfall and floods in future cities").

References

Antoniazza, G.: Bedload transport in Alpine streams: Lessons from newly-emerging monitoring systems, 2023.

Archer, D. and Stewart, D.: The installation and use of a snow pillow to monitor snow water equivalent, Water and environment journal, 9, 221–230, 1995.

Aune-Lundberg, L. and Strand, G.-H.: CORINE Land Cover 2006. The Norwegian CLC2006 project, Norsk institutt for skog og landskap, 2010.

Benettin, P., Soulsby, C., Birkel, C., Tetzlaff, D., Botter, G., and Rinaldo, A.: Using SAS functions and high-resolution isotope data to unravel travel time distributions in headwater catchments, Water Resources Research, 53, 1864–1878, 2017.

Benoit, L., Allard, D., and Mariethoz, G.: Stochastic rainfall modeling at sub-kilometer scale, Water Resources Research, 54, 4108–4130, 2018.

Beria, H., Larsen, J. R., Ceperley, N. C., Michelon, A., Vennemann, T., and Schaefli, B.: Understanding snow hydrological processes through the lens of stable water isotopes, Wiley Interdisciplinary Reviews: Water, 5, e1311, 2018.

Bloem, E., Forquet, N., Søiland, A., Binley, A., and French, H. K.: Towards understanding time-lapse electrical resistivity signals measured during contaminated snowmelt infiltration, Near Surface Geophysics, 18, 399–412, 2020.

Blott, S. J., Croft, D. J., Pye, K., Saye, S. E., and Wilson, H. E.: Particle size analysis by laser diffraction, Geological Society, London, Special Publications, 232, 63–73, 2004.

Braud, I., De Condappa, D., Soria, J. M., Haverkamp, R., Angulo-Jaramillo, R., Galle, S., and Vauclin, M.: Use of scaled forms of the infiltration equation for the estimation of unsaturated soil hydraulic properties (the Beerkan method), European Journal of Soil Science, 56, 361–374, 2005.

Brooks, R. H. and Corey, A. T.: Properties of porous media affecting fluid flow, Journal of the irrigation and drainage division, 92, 61–88, 1966.

Burdine, N.: Relative permeability calculations from pore size distribution data, Journal of Petroleum Technology, 5, 71–78, 1953.

Carey, S. K. and Woo, M.-k.: Slope runoff processes and flow generation in a subarctic, subalpine catchment, Journal of hydrology, 253, 110–129, 2001.

Carroll, R. W., Deems, J. S., Niswonger, R., Schumer, R., and Williams, K. H.: The importance of interflow to groundwater recharge in a snowmelt-dominated headwater basin, Geophysical Research Letters, 46, 5899–5908, 2019.

Ceperley, N., Zuecco, G., Beria, H., Carturan, L., Michelon, A., Penna, D., Larsen, J., and Schaefli, B.: Seasonal snow cover decreases young water fractions in high Alpine catchments, Hydrological processes, 34, 4794–4813, 2020.

Cianfrani, C., Buri, A., Vittoz, P., Grand, S., Zingg, B., Verrecchia, E., and Guisan, A.: Spatial modelling of soil water holding capacity improves models of plant distributions in mountain landscapes, Plant and Soil, 438, 57–70, 2019.

Clapp, R. B. and Hornberger, G. M.: Empirical equations for some soil hydraulic properties, Water resources research, 14, 601–604, 1978.

Corripio, J. G. and Corripio, M. J. G.: Package 'insol', 2019.

Cosby, B., Hornberger, G., Clapp, R., and Ginn, T.: A statistical exploration of the relationships of soil moisture characteristics to the physical properties of soils, Water resources research, 20, 682–690, 1984.

Desilets, D.: Calibrating a non-invasive cosmic ray soil moisture probe for snow water equivalent, Hydroinnova Technical Document 17-01, doi: 10.5281/zenodo. 439105, Hydroinnova Technical Document, pp. 17–01, 2017.

Eeckman, J.: Soil study results at Vallon de Nant : Soil moisture and soil temperature time series and granulometry results, https://doi.org/10.5281/zenodo.10136586, 2023.

Eeckman, J.: Liquid water content, ice water content and density measured via the SnowMelt Instrument at Auberge station, https://doi.org/10.5281/zenodo.11580271, 2024.

420 Fang, Z., Carroll, R. W., Schumer, R., Harman, C., Wilusz, D., and Williams, K. H.: Streamflow partitioning and transit time distribution in snow-dominated basins as a function of climate, Journal of Hydrology, 570, 726–738, 2019.

Fischer, A. M., Strassmann, K. M., Croci-Maspoli, M., Hama, A. M., Knutti, R., Kotlarski, S., Schär, C., Poberaj, C. S., Ban, N., Bavay, M., et al.: Climate scenarios for Switzerland CH2018–approach and implications, Climate services, 26, 100 288, 2022.

French, H. and Binley, A.: Snowmelt infiltration: monitoring temporal and spatial variability using time-lapse electrical resistivity, Journal

425 of Hydrology, 297, 174–186, 2004.

Fuentes, C., Vauclin, M., Parlange, J.-Y., and Haverkamp, R.: Soil-water conductivity of a fractal soil, in: Revival: Fractals in Soil Science (1998), pp. 333–340, CRC press, 2017.

Gance, J., Malet, J.-P., Supper, R., Sailhac, P., Ottowitz, D., and Jochum, B.: Permanent electrical resistivity measurements for monitoring water circulation in clayey landslides, Journal of Applied Geophysics, 126, 98–115, 2016.

430 Grand, S., Rubin, A., Verrecchia, E. P., and Vittoz, P.: Variation in soil respiration across soil and vegetation types in an alpine valley, Plos One, 11, e0163 968, 2016.

Hall, D. K., Nghiem, S. V., Schaaf, C. B., DiGirolamo, N. E., and Neumann, G.: Evaluation of surface and near-surface melt characteristics on the Greenland ice sheet using MODIS and QuikSCAT data, Journal of Geophysical Research: Earth Surface, 114, 2009.

Haverkamp, R., Ross, P., Smettem, K., and Parlange, J.: Three-dimensional analysis of infiltration from the disc infiltrometer: 2. Physically

435 based infiltration equation, Water Resources Research, 30, 2931–2935, 1994.

He, Z., Parajka, J., Tian, F., and Blöschl, G.: Estimating degree-day factors from MODIS for snowmelt runoff modeling, Hydrology and Earth System Sciences, 18, 4773–4789, 2014.

Heidbüchel, I., Troch, P. A., Lyon, S. W., and Weiler, M.: The master transit time distribution of variable flow systems, Water Resources Research, 48, https://doi.org/https://doi.org/10.1029/2011WR011293, 2012.

440 Hubbart, J., Link, T., Campbell, C., and Cobos, D.: Evaluation of a low-cost temperature measurement system for environmental applications, Hydrological Processes: an International Journal, 19, 1517–1523, 2005.

Kampf, S., Markus, J., Heath, J., and Moore, C.: Snowmelt runoff and soil moisture dynamics on steep subalpine hillslopes, Hydrological Processes, 29, 712–723, 2015.

Kattelmann, R.: Snowmelt lysimeters in the evaluation of snowmelt models, Annals of Glaciology, 31, 405–410, 2000.

445 KIT: Hydroinnova SnowFox Manual, snowFox Startup Guide, 2015.

Klaus, J. and McDonnell, J.: Hydrograph separation using stable isotopes: Review and evaluation, Journal of hydrology, 505, 47–64, 2013.

Kundzewicz, Z. W., Kanae, S., Seneviratne, S. I., Handmer, J., Nicholls, N., Peduzzi, P., Mechler, R., Bouwer, L. M., Arnell, N., Mach, K., et al.: Flood risk and climate change: global and regional perspectives, Hydrological Sciences Journal, 59, 1–28, 2014.

Lassabatère, L., Angulo-Jaramillo, R., Soria Ugalde, J., Cuenca, R., Braud, I., and Haverkamp, R.: Beerkan estimation of soil transfer

450 parameters through infiltration experiments—BEST, Soil science society of America journal, 70, 521–532, 2006.

Legros, J.: Soils of Alpine mountains, in: Developments in Earth Surface Processes, vol. 2, pp. 155–181, Elsevier, 1992.

Lorenzi, V., Banzato, F., Barberio, M. D., Goeppert, N., Goldscheider, N., Gori, F., Lacchini, A., Manetta, M., Medici, G., Rusi, S., et al.: Tracking flowpaths in a complex karst system through tracer test and hydrogeochemical monitoring: Implications for groundwater protection (Gran Sasso, Italy), Heliyon, 10, 2024.

455 Martinec, J.: Snowmelt-runoff model for stream flow forecasts, Hydrology Research, 6, 145–154, 1975.

Masson-Delmotte, V., Zhai, P., Pirani, S., Connors, C., Péan, S., Berger, N., Caud, Y., Chen, L., Goldfarb, M., and Scheel Monteiro, P. M.: Ipcc, 2021: Summary for policymakers. in: Climate change 2021: The physical science basis. contribution of working group i to the sixth assessment report of the intergovernmental panel on climate change, 2021.

Meeks, J., Moeck, C., Brunner, P., and Hunkeler, D.: Infiltration under snow cover: Modeling approaches and predictive uncertainty, Journal 460 of Hydrology, 546, 16–27, 2017.

Michelon, A., Ceperley, N., Beria, H., Larsen, J., Vennemann, T., and Schaefli, B.: Studying the dynamic of a high alpine catchment based on multiple natural tracers, Hydrology and Earth System Sciences Discussions, 2022, 1–43, 2022.

Michelon, A., Ceperley, N. C., Beria, H., Larsen, J., Vennemann, T., and Schaefli, B.: Hydrodynamics of a high Alpine catchment characterized by four natural tracers, Hydrology and earth system sciences, 27, 1403–1430, 2023.

465 Perret, A. and Martin, S.: Carte géomorphologique du vallon de Nant et étude de la marge proglaciaire du glacier des Martinets, 2015.

Pletterbauer, F., Melcher, A., and Graf, W.: Climate change impacts in riverine ecosystems, Riverine Ecosystem Management. Aquatic Ecology Series, 8, 203–223, 2018.

Reusser, D. E. and Zehe, E.: Low-cost monitoring of snow height and thermal properties with inexpensive temperature sensors, Hydrological Processes, 25, 1841–1852, 2011.

470 Rulin, O., Liliang, R., Weiming, C., and Zhongbo, Y.: Application of hydrological models in a snowmelt region of Aksu River Basin, Water Science and Engineering, 1, 1–13, 2008.

Santos, A. C., Portela, M. M., Rinaldo, A., and Schaefli, B.: Analytical flow duration curves for summer streamflow in Switzerland, Hydrology and Earth System Sciences, 22, 2377–2389, https://doi.org/10.5194/hess-22-2377-2018, 2018.

Schaefli, B., Nicótina, L., Imfeld, C., Da Ronco, P., Bertuzzo, E., and Rinaldo, A.: SEHR-ECHO v1. 0: a Spatially Explicit Hydrologic 475 Response model for ecohydrologic applications, Geoscientific Model Development, 7, 2733–2746, 2014.

Sommertechnik: Snow Pack Analyser (SPA), Examples, http://www.sommer.at, document release: V1.0.0, 2009.

Thornton, J. M.: Fully-integrated hydrological modelling in steep, snow-dominated, geologically complex Alpine terrain, Ph.D. thesis, PhD thesis, University of Neuchâtel, Switzerland, https://files. osf. io/v1 . . . , 2020.

Thornton, J. M., Mariethoz, G., and Brunner, P.: A 3D geological model of a structurally complex Alpine region as a basis for interdisciplinary 480 research, Scientific data, 5, 1–20, 2018.

Thornton, J. M., Brauchli, T., Mariethoz, G., and Brunner, P.: Efficient multi-objective calibration and uncertainty analysis of distributed snow simulations in rugged alpine terrain, Journal of Hydrology, 598, 126 241, 2021.

Thornton, J. M., Therrien, R., Mariéthoz, G., Linde, N., and Brunner, P.: Simulating fully-integrated hydrological dynamics in complex alpine headwaters: potential and challenges, Water Resources Research, 58, e2020WR029 390, 2022.

485 Van Genuchten, M. T.: A closed-form equation for predicting the hydraulic conductivity of unsaturated soils, Soil science society of America journal, 44, 892–898, 1980.

Vionnet, V., Brun, E., Morin, S., Boone, A., Faroux, S., Le Moigne, P., Martin, E., and Willemet, J.: The detailed snowpack scheme Crocus and its implementation in SURFEX v7, Geoscientific Model Development Discussions, 4, 2365–2415, 2011.

Webb, R., Williams, M. W., and Erickson, T. A.: The spatial and temporal variability of meltwater flow paths: Insights from a grid of over
490   100 snow lysimeters, Water Resources Research, 54, 1146–1160, 2018a.

Webb, R. W., Fassnacht, S. R., and Gooseff, M. N.: Hydrologic flow path development varies by aspect during spring snowmelt in complex
    subalpine terrain, The Cryosphere, 12, 287–300, https://doi.org/10.5194/tc-12-287-2018, 2018b.

Wilusz, D., Harman, C., Ball, W., Maxwell, R., and Buda, A.: Using particle tracking to understand flow paths, age distributions, and the
    paradoxical origins of the inverse storage effect in an experimental catchment, Water Resources Research, 56, e2019WR025 140, 2020.

495 Zhang, F., Zhang, H., Hagen, S. C., Ye, M., Wang, D., Gui, D., Zeng, C., Tian, L., and Liu, J.: Snow cover and runoff modelling in a high
    mountain catchment with scarce data: effects of temperature and precipitation parameters, Hydrological processes, 29, 52–65, 2015.